Supplementary Information

Zr doped mesoporous $LaTaON_2$ for efficient photocatalytic water splitting

Yawei Wang[a,c]‡, Shu Jin[a]‡, Guoxiang Pan[b], Zuxin Li[b], Long Chen[c], Gang Liu*[d] and Xiaoxiang Xu,*[a,b,c]

[a]Clinical and Central Lab, Putuo People's Hospital, Tongji University, 1291 Jiangning Road, Shanghai, 200060, China

[b]Department of Materials Engineering, Huzhou University, Huzhou 313000,China

*[c]Shanghai Key Lab of Chemical Assessment and Sustainability, School of Chemical Science and Engineering, Tongji University, 1239 Siping Road, Shanghai, 200092, China, *Email: xxxu@tongji.edu.cn, telephone: +86-21-65986919*

*[d]Shenyang National laboratory for Materials Science, Institute of Metal Research, Chinese Academy of Science, 72 Wenhua Road, Shenyang 110016, China, *Email: gangliu@imr.ac.cn*

‡ These authors contribute equally.

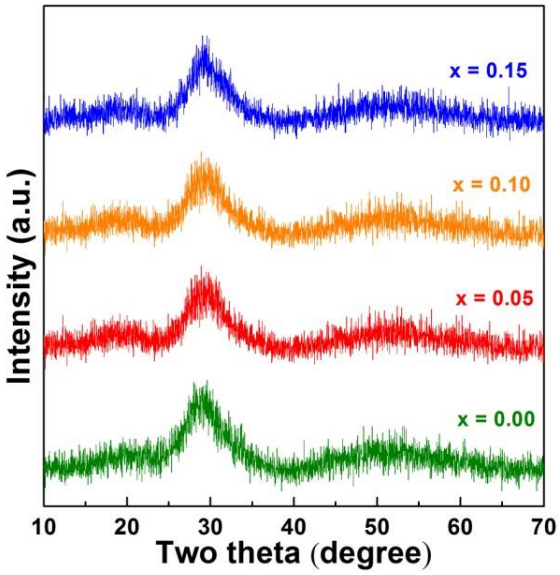

Figure S1. X-ray powder diffraction patterns of all oxide precursors.

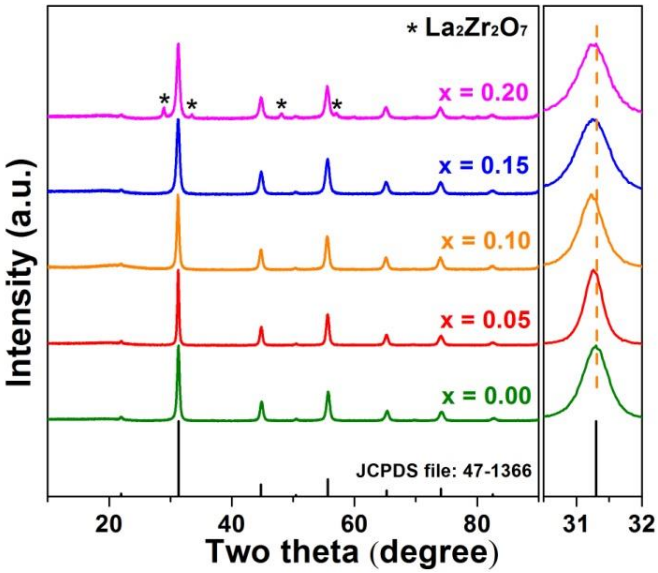

Figure S2. X-ray powder diffraction patterns of $LaTa_{1-x}Zr_xO_{1+y}N_{2-y}$ ($0 \leq x \leq 0.20$), peaks of $La_2Zr_2O_7$ are marked by asterisks (*).

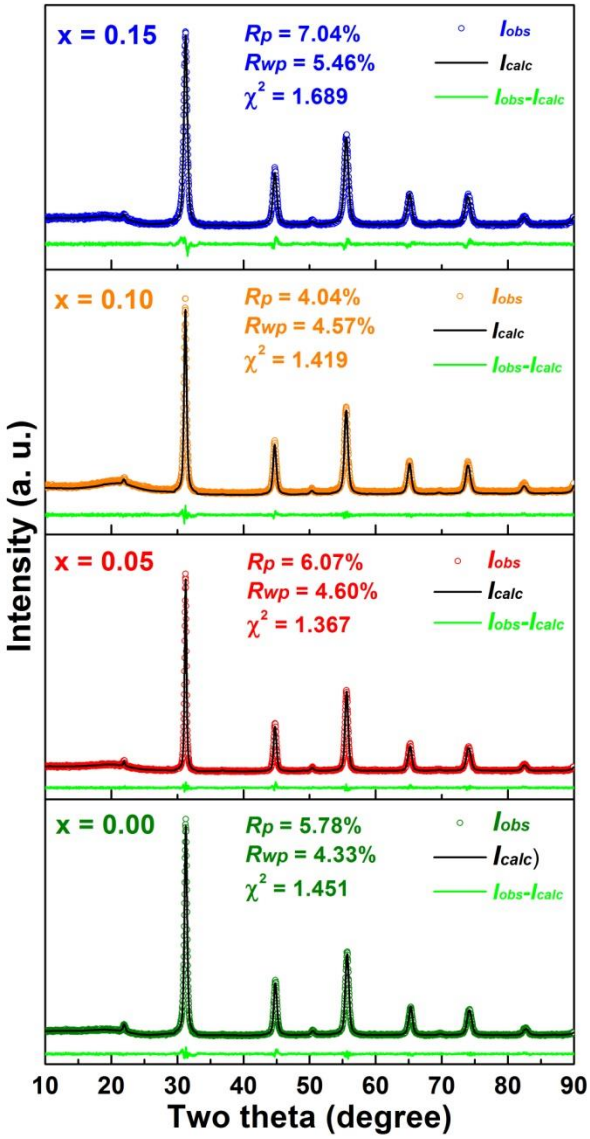

Figure S3. Observed and calculated X-ray powder diffraction patterns of all samples using the *I2/m* space group, the refinement converges with good *R* and χ^2 factor values of all samples are inserted.

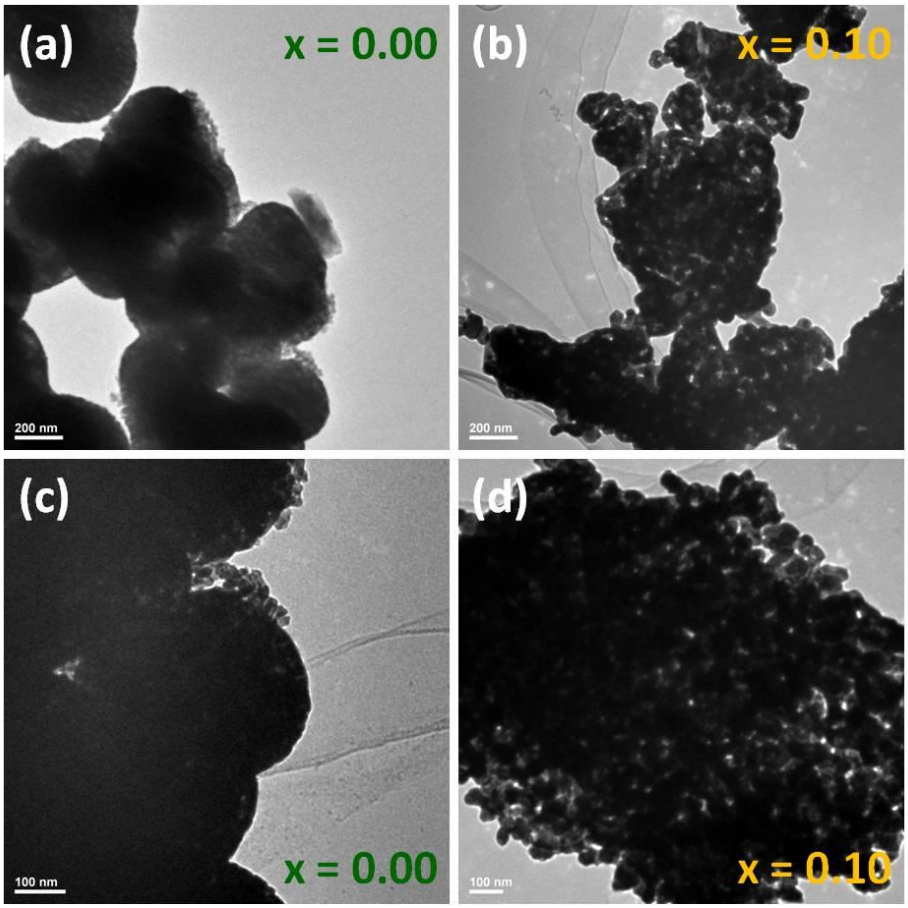

Figure S4. TEM images of freshly prepared sample powders of (a, c) pristine $LaTaON_2$ (x = 0.00) and (b, d) $LaTa_{0.9}Zr_{0.1}O_{1+y}N_{2-y}$ (x = 0.10) at different magnifications.

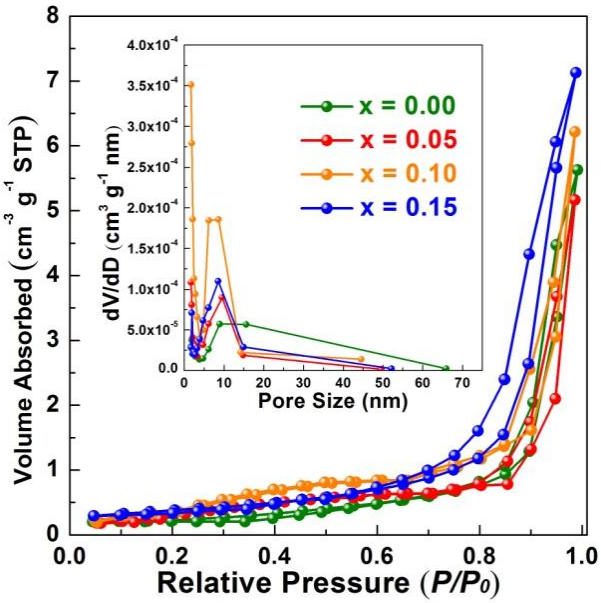

Figure S5. Nitrogen adsorption-desorption isotherms of freshly prepared sample powders $LaTa_{1-x}Zr_xO_{1+y}N_{2-y}$ ($0 \leq x \leq 0.15$), the pore-size distribution curves is inserted.

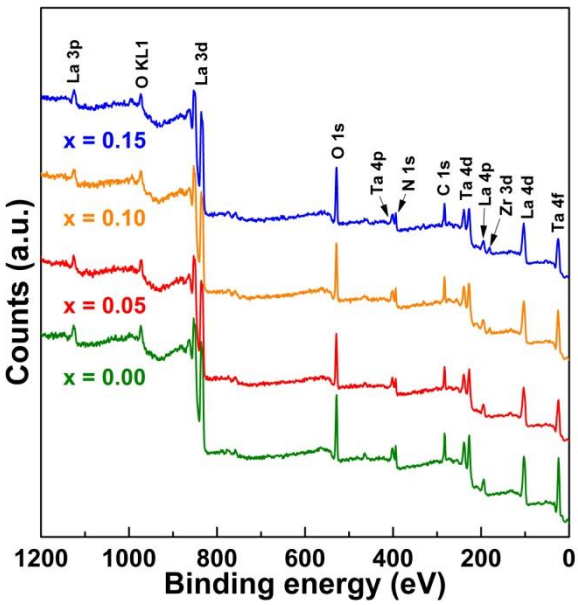

Figure S6. XPS survey spectra of all samples.

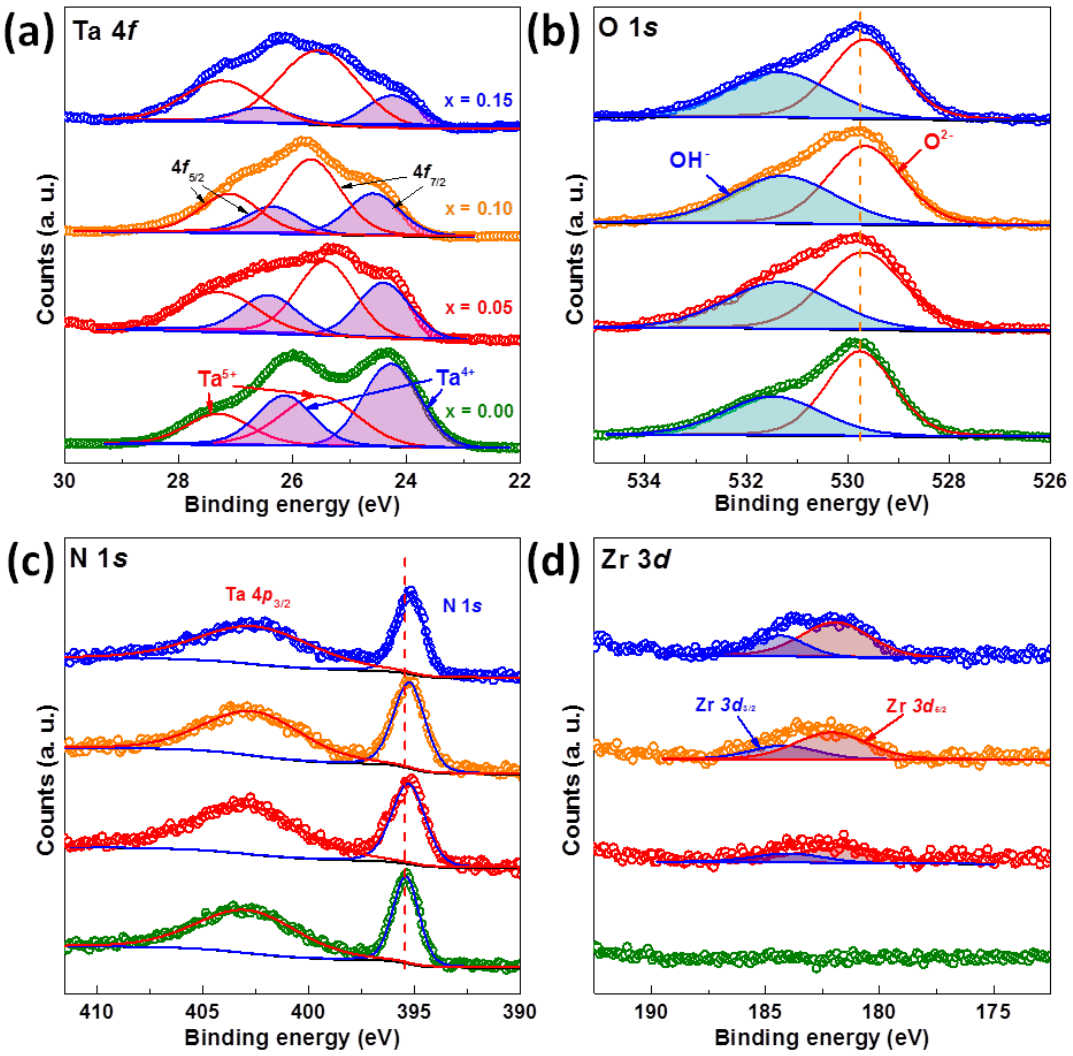

Figure S7. X-ray photoelectron spectra of core-level electrons of constituent elements in all sample powders $LaTa_{1-x}Zr_xO_{1+y}N_{2-y}$ ($0 \leq x \leq 0.15$): (a) Ta 4*f*; (b) O 1*s*; (c) N *1s*; (d) Zr 3*d*.

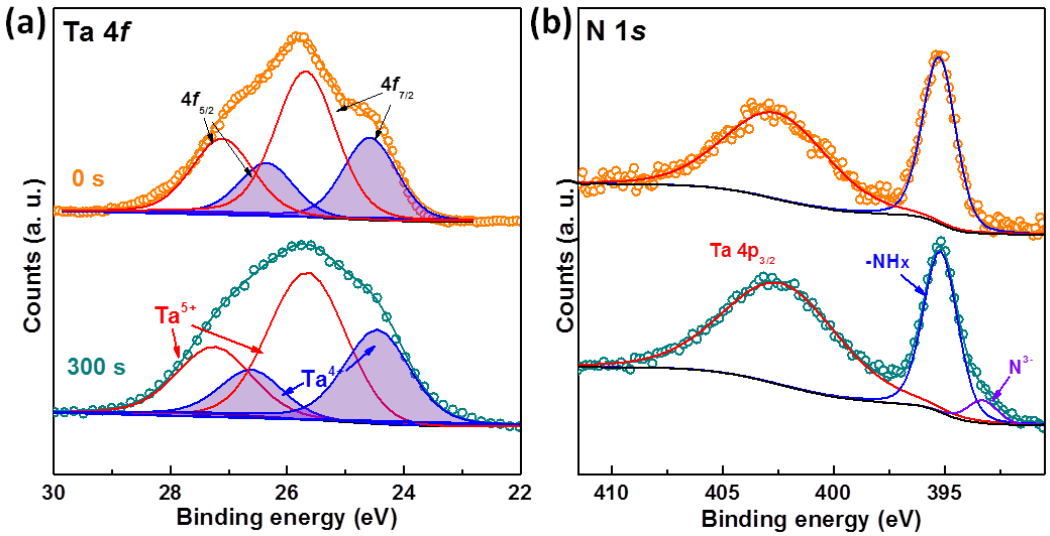

Figure S8. X-ray photoelectron spectra of (a) Ta 4*f* and (b) N 1*s* state *after in* situ Ar ion sputtering $LaTa_{0.9}Zr_{0.1}O_{1+y}N_{2-y}$ (x = 0.10) with beam energy of 4 keV for 300 s.

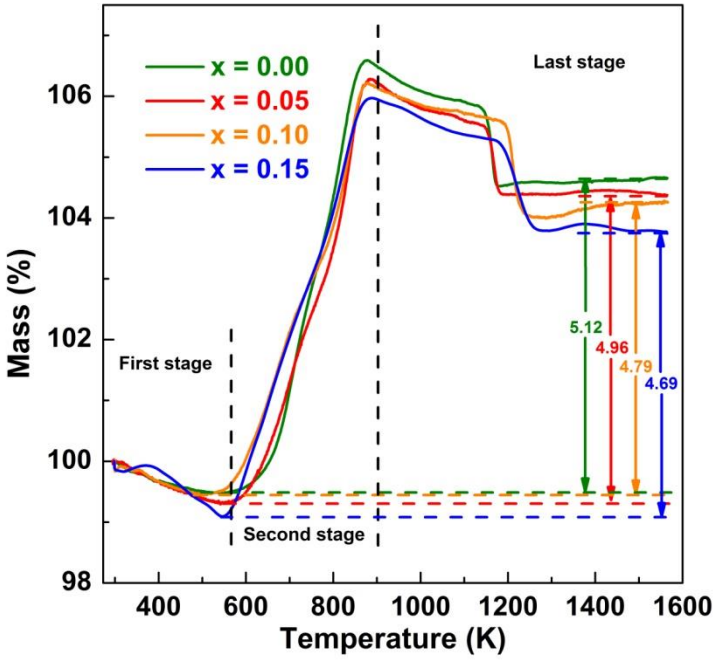

Figure S9. TG curves of $LaTa_{1-x}Zr_xO_{1+y}N_{2-y}$ ($0 \leq x \leq 0.15$) powders in air with heating rate of 10 K min^{-1} from 273 K to 1573 K. All TGA curves can be divided into three regions like previous reports [1-4].

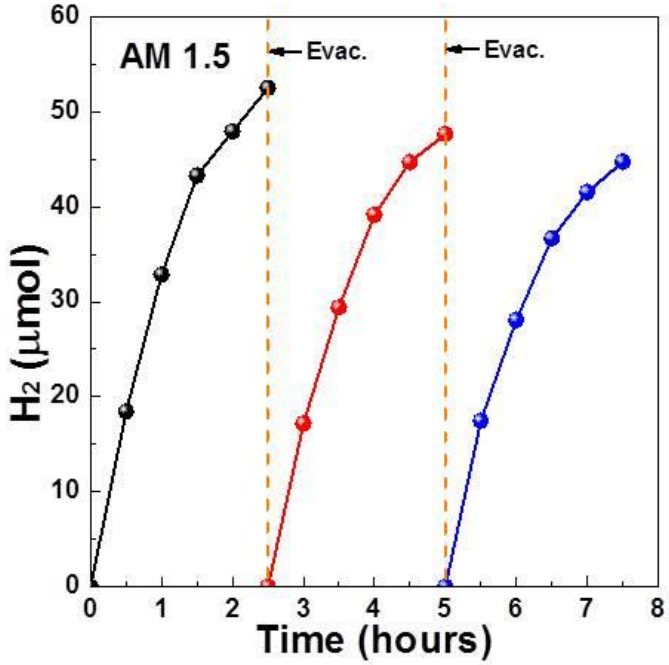

Figure S10. Time courses of hydrogen evolution on $LaTa_{0.9}Zr_{0.1}O_{1+y}N_{2-y}$ (x = 0.10) under AM 1.5 irradiation.

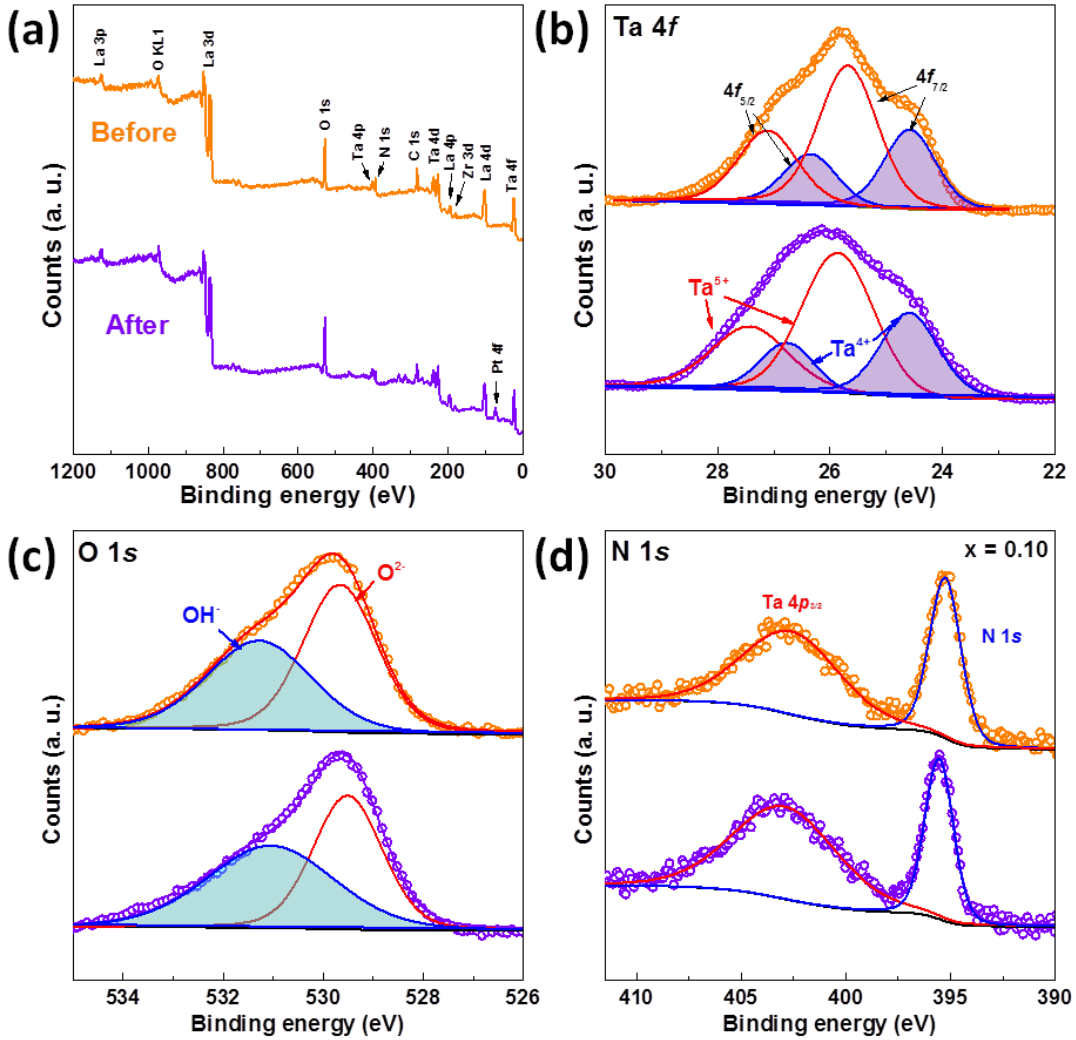

Figure S11. (a) XPS survey spectra and X-ray photoelectron spectra of (b) Ta 4*f*; (c) O 1*s*; (d) N 1*s* in $LaTa_{0.9}Zr_{0.1}O_{1+y}N_{2-y}$ (x = 0.10) before and after photocatalytic water reduction reaction.

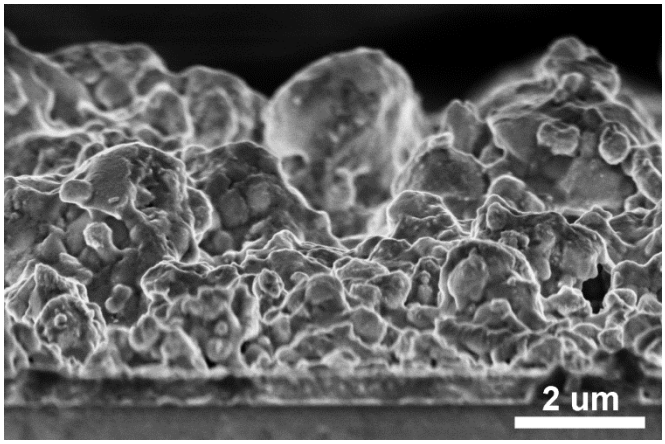

Figure S12. Field emission scanning electron microcopy image of $LaTa_{0.9}Zr_{0.1}O_{1+y}N_{2-y}$ (x = 0.10) electrode.

Table S1. The refined atomic coordinates and site occupancies of as-prepared samples $LaTa_{1-x}Zr_xO_{1+y}N_{2-y}$ ($0 \leq x \leq 0.15$)

Sample	Element	x	y	z	Occupancy
0.00	La1	0.7601(1)	0	0.2473(3)	1
	Ta1	0.75	0.25	0.75	1
	O1	0.7130(1)	0	0.6983(2)	0.63
	N1	0.7130(1)	0	0.6983(2)	0.37
	N2	0	0.7401(1)	0	1
	O2	0.5	0.2550(2)	0	0.37
	N3	0.5	0.2550(2)	0	0.63
0.05	La1	0.7591(2)	0	0.2479(2)	1
	Ta1	0.75	0.25	0.75	0.95
	Zr1	0.75	0.25	0.75	0.05
	O1	0.7112(3)	0	0.6985(2)	0.655
	N1	0.7112(3)	0	0.6985(2)	0.345
	N2	0	0.7561(3)	0	1
	O2	0.5	0.2630(1)	0	0.395
	N3	0.5	0.2630(1)	0	0.605
0.10	La1	0.7597(2)	0	0.2475(1)	1
	Ta1	0.75	0.25	0.75	0.9
	Zr1	0.75	0.25	0.75	0.1
	O1	0.7123(3)	0	0.6986(4)	0.68

	N1	0.7123(3)	0	0.6986(4)	0.32
	N2	0	0.7432(1)	0	1
	O2	0.5	0.2608(7)	0	0.42
	N3	0.5	0.2608(7)	0	0.58
	La1	0.7587(1)	0	0.2483(3)	1
	Ta1	0.75	0.25	0.75	0.85
	Zr1	0.75	0.25	0.75	0.15
0.15	O1	0.7070(2)	0	0.6989(3)	0.7050
	N1	0.7070(2)	0	0.6989(3)	0.2950
	N2	0	0.7531(2)	0	1
	O2	0.5	0.2650(2)	0	0.445
	N3	0.5	0.2650(2)	0	0.555

Table S2. Surface elemental compositions measured by XPS for as-prepared samples.

x	La (at.%)	Ta (at.%)	Zr (at.%)	O (at.%)	N (at.%)	O/N
0.00	19.04	14.79	-	50.94	15.23	3.34
0.05	19.12	14.35	1.25	50.28	15.00	3.35
0.10	18.77	14.25	2.19	50.12	14.67	3.41
0.15	19.40	13.92	2.72	51.37	12.59	4.08

Table S3. The binding energy (BE), peak area ratio (PAR) and full width at half maximum (FWHM) of Ta $4f_{7/2}$ and $4f_{5/2}$ by peak-fitting XPS spectra in all samples

x	Ta $4f_{5/2}$			Ta $4f_{7/2}$		
	BE (eV)	PAR (%)	FWHM (eV)	BE (eV)	PAR (%)	FWHM (eV)
0.00	27.33 / 26.12	18.49 / 24.36	1.33 / 1.34	25.51 / 24.25	24.66 / 32.49	1.43 / 1.45
0.05	27.36 / 26.47	25.00 / 17.85	1.45 / 1.32	25.68 / 24.55	33.34 / 23.81	1.34 / 1.35
0.10	27.10 / 26.36	31.23 / 11.63	1.35 / 1.27	25.69 / 24.60	41.63 / 15.51	1.37 / 1.23
0.15	27.25 / 26.54	33.75 / 9.11	1.55 / 1.25	25.55 / 24.28	45.00 / 12.14	1.58 / 1.26
After	27.43 / 26.77	28.44 / 14.42	1.51 / 1.23	25.86 / 24.60	37.92 / 19.22	1.53 / 1.24
300 s	27.28 / 26.65	27.10 / 15.76	1.54 / 1.34	25.69 / 24.46	36.13 / 21.01	1.56 / 1.36

Table S4. Expected and measured mass changes of as-prepared samples $LaTa_{1-x}Zr_xO_{1+y}N_{2-y}$ ($0 \leq x \leq 0.15$).

x	Expected mass changes	Measured mass changes
0.00	5.49%	5.12%
0.05	5.43%	4.96%
0.10	5.34%	4.79%
0.15	5.27%	4.69%

References

1. Y. W. Wang, D. Z. Zhu and X. X. Xu, *ACS Appl. Mater. Interfaces*, 2016, **8**, 35407-35418.
2. D. Li, W. J. Li, C. Fasel, J. Shen and R. Riedel, *J. Alloy. Compd.*, 2014, **586**, 567-573.
3. A. Rachel, S. G. Ebbinghaus, M. Gungerich, P. J. Klar, J. Hanss, A. Weidenkaff and A. Reller, *Thermochim. Acta*, 2005, **438**, 134-143.
4. R. Aguiar, D. Logvinovich, A. Weidenkaff, A. Reller and S. G. Ebbinghaus, *Thermochim. Acta*, 2008, **471**, 55-60.